



Reduction of one-dimensional non-Hermitian point-gap topology by interactionsTsuneya Yoshida  and Yasuhiro Hatsugai *Department of Physics, University of Tsukuba, Ibaraki 305-8571, Japan*

(Received 19 May 2022; revised 18 July 2022; accepted 31 October 2022; published 28 November 2022)

In spite of extensive works on non-Hermitian topology, interaction effects remain crucial questions. We analyze correlated non-Hermitian systems with special emphasis on the one-dimensional point-gap topology. Specifically, our analysis elucidates that interactions result in a reduction of the topological classification $\mathbb{Z} \times \mathbb{Z} \rightarrow \mathbb{Z}$ for systems of one synthetic dimension with charge $U(1)$ symmetry and spin-parity symmetry. Furthermore, we analyze an extended Hatano-Nelson chain which exhibits striking interaction effects; interactions destroy the non-Hermitian skin effect at the noninteracting level. This fragility of the non-Hermitian skin effect against interactions is consistent with the reduction of the point-gap topology in the one spatial dimension. The above discoveries shed light on the topology of correlated systems and open up different directions for research on non-Hermitian topological physics.

DOI: [10.1103/PhysRevB.106.205147](https://doi.org/10.1103/PhysRevB.106.205147)**I. INTRODUCTION**

Topological insulators and superconductors have been extensively analyzed for these 15 years [1–9]. In particular, considerable efforts have been devoted to understanding interaction effects on nontrivial topology, which has revealed a variety of unique phenomena. For instance, interaction effects induce topological ordered phases [10–16] which host anyons. In addition, it has turned out that interaction effects change the \mathbb{Z} classification of topological superconductors at the mean-field level to the \mathbb{Z}_8 classification [17]. Such a reduction phenomenon of possible topological phases for a given symmetry class has been theoretically reported for arbitrary spatial dimensions [18–32]. Furthermore, a theoretical work [33] elucidated that the reduction can also occur in synthetic dimensions which are considered to be fabricated in cold atoms [34–37]. These developments reveal the ubiquity of the reduction phenomena.

Along with the above significant progress, understanding of the non-Hermitian band topology rapidly developed in recent years [38–43]. Remarkably, it has been elucidated that the point-gap topology induces novel phenomena which do not have Hermitian counterparts [44–55]. A prime example is the emergence of the exceptional points [56–60] (and their symmetry-protected variants [61–69]) at which the point-gap topology induces band touching for both the real and imaginary parts. Another remarkable phenomenon is a non-Hermitian skin effect which results in extreme sensitivity to the presence or absence of boundaries [46,70–76]. So far, the non-Hermitian topological band theory has been applied to a wide range of systems from quantum [77–87] to classical [88–102] systems.

While most studies have focused on the noninteracting cases so far, interaction effects on non-Hermitian topology are attracting growing interest [103–122] due to the potential presence of novel non-Hermitian phenomena. Such interest in interaction effects on non-Hermitian topology is further enhanced by the recent development of technology in cold

atoms which allows us to experimentally tune both dissipation and two-body interactions [123,124]. Despite these efforts, the current understanding of point-gap topology in correlated systems is quite limited. In particular, knowledge about the reduction of point-gap topology is limited only to the zero dimension [125], which poses the following significant question: fate of higher-dimensional point-gap topology under interactions.

We herein address a primitive version of the above question. Specifically, we analyze the fate of one-dimensional point-gap topology in both cases of synthetic and spatial dimensions. We start with the topology in one synthetic dimension. Our analysis reveals the reduction of $\mathbb{Z} \times \mathbb{Z} \rightarrow \mathbb{Z}$ for systems with charge $U(1)$ symmetry and spin-parity symmetry. We end up with this conclusion by analyzing a toy model, as well as by using an argument in terms of topological invariants. Furthermore, we analyze an extended Hatano-Nelson chain in which such a reduction results in a striking phenomenon: the fragility of a non-Hermitian skin effect against interactions in one spatial dimension.

The rest of this paper is organized as follows. In Sec. II, we discuss the reduction of the non-Hermitian topological classification in one synthetic dimension by introducing topological invariants. In Sec. III, computing the obtained topological invariants, we address the reduction of the topological classification in one spatial dimension. A brief summary and discussion are provided in Sec. IV. In Appendix A, a detailed analysis of a non-Hermitian quantum dot is provided. Appendix B is devoted to a detailed analysis of the extended Hatano-Nelson chain.

II. POINT-GAP TOPOLOGY IN ONE SYNTHETIC DIMENSION**A. Topological invariants**

First, we provide a generic argument in terms of topological invariants. Consider a quantum dot whose many-body

Hamiltonian reads

$$\hat{H} = \hat{H}_0(\theta) + \hat{H}_{\text{int}}, \quad (1)$$

with $\hat{H}_0(\theta) = \sum_{\alpha\beta} \hat{\Psi}_\alpha^\dagger h_{\alpha\beta}(\theta) \hat{\Psi}_\beta$ and $\hat{\Psi}^T = (\hat{c}_{a\uparrow}, \hat{c}_{a\downarrow}, \hat{c}_{b\uparrow}, \hat{c}_{b\downarrow}, \dots)$. The second term, \hat{H}_{int} , denotes two-body interactions of fermions. Here, the one-body Hamiltonian $h(\theta)$ is non-Hermitian and satisfies $h(2\pi) = h(0)$. The synthetic dimension is parameterized by θ , which corresponds to a tunable parameter in experiments [126,127] (e.g., a hopping integral in cold atoms). The operator $\hat{c}_{l\sigma}^\dagger$ ($\hat{c}_{l\sigma}$) creates (annihilates) a fermion in orbital l ($l = a, b, \dots$) and spin state σ ($\sigma = \uparrow, \downarrow$). The subscript α labels the set of l and σ .

Throughout this paper, we suppose that the Hamiltonian (1) respects the charge U(1) symmetry and spin-parity symmetry. Namely, the zero-dimensional Hamiltonian satisfies

$$[\hat{H}, \hat{N}] = 0, \quad [\hat{H}, e^{i\pi\hat{S}^z}] = 0, \quad (2)$$

with $\hat{N} = \sum_\alpha \hat{\Psi}_\alpha^\dagger \hat{\Psi}_\alpha$ and $\hat{S}^z = \sum_{l=a,b,\dots} (\hat{c}_{l\uparrow}^\dagger \hat{c}_{l\uparrow} - \hat{c}_{l\downarrow}^\dagger \hat{c}_{l\downarrow})/2$.

Here, let us discuss the point-gap topology of the above system. In terms of the one-body Hamiltonian, we can introduce two distinct \mathbb{Z} invariants due to the spin-parity symmetry. Because the one-body Hamiltonian $h(\theta)$ is periodic in θ , we can introduce the winding number w :

$$w = \int_0^{2\pi} \frac{d\theta}{2\pi i} \partial_\theta \text{tr} \ln [h(\theta) - \epsilon_{\text{ref}} \mathbb{1}], \quad (3)$$

with the reference energy $\epsilon_{\text{ref}} \in \mathbb{C}$. The derivative with respect to θ is denoted by ∂_θ . Here, tr denotes the trace of a matrix (i.e., $\text{tr}h = \sum_\alpha h_{\alpha\alpha}$).

In addition, we can introduce the spin winding number w_s :

$$w_s = \int_0^{2\pi} \frac{d\theta}{4\pi i} \partial_\theta \text{tr} \{s^z \ln [h(\theta) - \epsilon_{\text{ref}} \mathbb{1}]\}, \quad (4)$$

with $(s^z)_{\alpha\beta} = \text{sgn}(\sigma) \delta_{\alpha\beta}$. Here, $\delta_{\alpha\beta}$ takes a value of 1 (0) for $\alpha = \beta$ ($\alpha \neq \beta$), and $\text{sgn}(\sigma)$ takes a value of 1 (−1) for $\sigma = \uparrow$ (\downarrow). For the spin winding number the spin-parity symmetry is essential; the one-body Hamiltonian satisfies $[s^z, h(\theta)] = 0$ in the presence of the spin-parity symmetry [128].

The above results indicate that in the presence of the U(1) symmetry and the spin-parity symmetry, the point-gap topology of $h(\theta)$ is characterized by two distinct \mathbb{Z} invariants.

Now, let us discuss the point-gap topology of the many-body Hamiltonian. In the presence of the spin-parity symmetry, the Hamiltonian \hat{H} can be block diagonalized with \hat{N} and $\hat{P} := (-1)^{\hat{N}_\uparrow} = e^{i\frac{\pi}{2}\hat{N}} e^{i\pi\hat{S}^z}$. Here, \hat{N}_\uparrow denotes the operator of the total number of fermions in the up-spin state. Therefore, for each Fock space, the following many-body winding number $W_{(N,P)}$ can be introduced [129]:

$$W_{(N,P)}(E_{\text{ref}}) = \int_0^{2\pi} \frac{d\theta}{2\pi i} \partial_\theta \text{Tr} \ln [\hat{H}_{(N,P)} - E_{\text{ref}} \mathbb{1}], \quad (5)$$

where N and P are eigenvalues of \hat{N} and \hat{P} , respectively. The reference energy is denoted by $E_{\text{ref}} \in \mathbb{C}$. By $\hat{H}_{(N,P)}$, we denote the many-body Hamiltonian for the subsector with (N, P) . Here, Tr denotes the trace over the subsector of the Fock space.

In the absence of interactions, eigenvalues of the many-body Hamiltonian $\hat{H}_{(N,P)}$ for each Fock space are computed

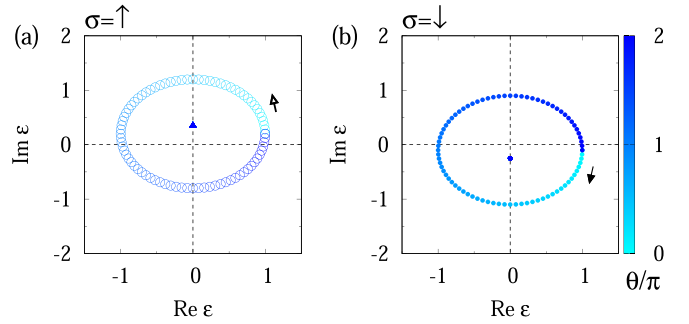


FIG. 1. Spectral flow of the one-body Hamiltonian $h(\theta)$. Data for the subsector with (a) $\sigma = \uparrow$ and (b) $\sigma = \downarrow$ are plotted. The color denotes the value of θ . The data are obtained for $(\lambda, \epsilon_{a\uparrow}, \epsilon_{a\downarrow}, \epsilon_{b\uparrow}, \epsilon_{b\downarrow}) = (1, 0.2, -0.1, 0.35, -0.25)$.

from the eigenvalues of the one-body Hamiltonian $h(\theta)$ whose point-gap topology is characterized by w and w_s .

The above results indicate that the point-gap topology of the one-body Hamiltonian $h(\theta)$ is characterized by a set of two \mathbb{Z} invariants (w, w_s) , while the topology of the many-body Hamiltonian \hat{H} is characterized by the \mathbb{Z} invariant $W_{(N,P)}$ for each sector of the Fock space. As we see below, this fact is consistent with the behavior that the nontrivial topology characterized by $(w, w_s) = (0, 1)$ is trivialized by introducing the interactions.

B. Two-orbital quantum dot: Noninteracting case

As a specific case of Eq. (1), let us consider a two-orbital quantum dot ($l = a, b$) with a diagonal matrix $h(\theta) [h_{\alpha\beta}(\theta) = h_\alpha(\theta) \delta_{\alpha\beta}]$ whose diagonal elements are written as

$$h_\alpha(\theta) = \lambda e^{i\theta} \delta_{\alpha,(a,\uparrow)} + \lambda e^{-i\theta} \delta_{\alpha,(a,\downarrow)} + i\epsilon_{l\sigma} \delta_{\alpha,(l,\sigma)}. \quad (6)$$

Here, λ and $\epsilon_{l\sigma}$ ($l = a, b$ and $\sigma = \uparrow, \downarrow$) are real numbers. At the noninteracting level, couplings between orbitals are absent. The one-body Hamiltonian of orbital a corresponds to the small cycle limit of an extended Hatano-Nelson chain under the twisted boundary condition [see Eq. (10)].

The topology of $h(\theta)$ is characterized as $(w, w_s) = (0, 1)$ for $\epsilon_{\text{ref}} = 0$ and $|\epsilon_{a\sigma}| < \lambda$ ($\sigma = \uparrow, \downarrow$). To be concrete, we plot a spectral flow of the one-body Hamiltonian in Fig. 1 for $(\lambda, \epsilon_{a\uparrow}, \epsilon_{a\downarrow}, \epsilon_{b\uparrow}, \epsilon_{b\downarrow}) = (1, 0.2, -0.1, 0.35, -0.25)$. Figure 1 indicates that as θ increases from 0 to 2π , an eigenvalue winds around the origin in the clockwise (counterclockwise) direction for subsector $\sigma = \uparrow$ ($\sigma = \downarrow$). The above numerical data support that the topology of $h(\theta)$ is characterized by $(w, w_s) = (0, 1)$.

Figure 2(a) displays a spectral flow of the many-body Hamiltonian \hat{H}_0 for the subsector with $(N, P) = (2, 1)$ in the Fock space. We can observe the loop structure of the spectral flow due to the topology of the one-body Hamiltonian $h(\theta)$. However, Fig. 2(a) indicates that $\hat{H}_{(2,1)}$ is topologically trivial (i.e., $W_{(2,1)} = 0$) for $E_{\text{ref}} = 0$ because one eigenvalue winds around the origin in the clockwise direction and the other eigenvalue winds around the origin in the opposite direction.

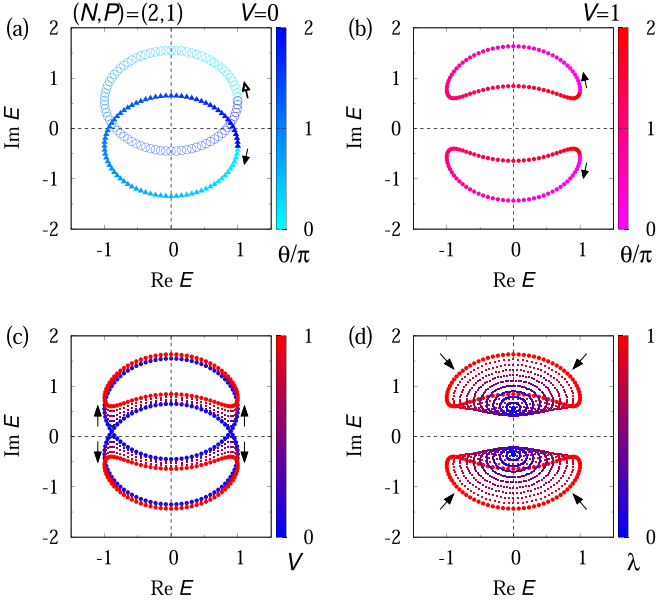


FIG. 2. Spectral flow of the many-body Hamiltonian for the subsector with $(N, P) = (2, 1)$. (a) Spectral flow for $J = V = 0$ and $\lambda = 1$. Data for the subsector with $(N, S^z) = (2, 1) [(2, -1)]$ are plotted with open circles (solid triangles). (b) Spectral flow for $V = J = \lambda = 1$. In (a) and (b), we can see that the eigenvalues flow as denoted by the arrows with θ increasing from 0 to 2π . (c) Spectral flow for several values of V ($J = V$) at $\lambda = 1$. With V increasing from 0 to 1, the eigenvalues flow as denoted by the arrows. (d) Spectral flow for several values of λ for $V = J = \sqrt{\lambda}$. With λ decreasing from 1 to 0, the eigenvalues flow as denoted by the arrows. The data are obtained for $(\epsilon_{a\uparrow}, \epsilon_{a\downarrow}, \epsilon_{b\uparrow}, \epsilon_{b\downarrow}) = (0.2, -0.1, 0.35, -0.25)$.

C. Two-orbital quantum dot: Interacting case

Now, let us introduce the following two-body interaction:

$$\hat{H}_{\text{int}} = \frac{iJ}{2}(\hat{S}_a^+ \hat{S}_b^- + \text{H.c.}) + \frac{iV}{2}(\hat{S}_a^+ \hat{S}_b^+ + \text{H.c.}), \quad (7)$$

with real numbers J and V . Here, H.c. denotes the Hermitian conjugate of the corresponding operator [e.g., $iJ(\hat{S}_a^+ \hat{S}_b^- + \text{H.c.}) = iJ(\hat{S}_a^+ \hat{S}_b^- + \hat{S}_a^- \hat{S}_b^+)$]. The spin operator \hat{S}_l^\pm is defined as $\hat{S}_l^\pm = \hat{S}_l^x \pm i\hat{S}_l^y$, with $\hat{S}_l^{x(y)}$ being the x (y) component of the spin operator for orbital l . The above two-body interactions respect charge $U(1)$ symmetry and spin-parity symmetry; applying the operator $e^{i\pi\hat{S}^z}$ transforms the spin operators as $e^{i\pi\hat{S}^z} \hat{S}_l^\pm e^{-i\pi\hat{S}^z} = -\hat{S}_l^\pm$, meaning that the interactions respect spin-parity symmetry.

For the sake of simplicity, we focus on the subsector with $(N, P) = (2, 1)$. The results for subsector $(N, P) = (2, -1)$ are provided in Sec. A 1. Figure 2(b) displays the spectral flow for $V = J = 1$. Remarkably, Fig. 2(b) indicates that the interactions open an imaginary gap; interactions split the loops which wind the origin at the noninteracting level [see Fig. 2(a)].

This fact indicates that interactions [Eq. (7)] allow a smooth deformation of the spectral flow for $\lambda = 1$ to that for $\lambda = 0$ without closing the point gap at $E_{\text{ref}} = 0$, the latter of which is obviously trivial. Indeed, the following deformation smoothly connects the Hamiltonian $\hat{H}(\theta)$ for $\lambda = 1$ and that

for $\lambda = 0$: (i) Increasing V from 0 to 1 for $\lambda = 1$ and $J = V$ [see Fig. 2(c)]; (ii) decreasing λ from 1 to 0 for $J = V = \sqrt{\lambda}$ [see Fig. 2(d)]. This deformation demonstrates that the many-body Hamiltonian $\hat{H}_{(2,1)}(\theta)$ is topologically trivial.

We note that the difference in the symmetry constraint of the spin-parity symmetry is essential for the imaginary gap at $\text{Im}E = 0$ in Fig. 2(b). As discussed above, the symmetry constraint (2), which results in $[s^z, h(\theta)] = 0$, forbids hybridization terms between two distinct subsectors with (N, S^z) . In contrast, the symmetry constraint allows such hybridization terms for two-body interactions \hat{H}_{int} . Therefore, the two-body interactions can destroy the loop structure arising from the nontrivial topology of the one-body Hamiltonian [see Figs. 2(a) and 2(b)].

For instance, in the subsector with $(N, P) = (2, 1)$, the Hamiltonian is written as

$$\hat{H}_{(2,1)} = \begin{pmatrix} \lambda e^{i\theta} + i\epsilon_{a\uparrow} + i\epsilon_{b\uparrow} & \frac{iV}{2} \\ \frac{iV}{2} & \lambda e^{-i\theta} + i\epsilon_{a\downarrow} + i\epsilon_{b\downarrow} \end{pmatrix}.$$

Here, we have chosen the following basis vectors spanning the subsector of the Fock space: $(\hat{c}_{a\uparrow}^\dagger \hat{c}_{b\uparrow}^\dagger |0\rangle, \hat{c}_{a\downarrow}^\dagger \hat{c}_{b\downarrow}^\dagger |0\rangle)$. The vacuum state is denoted by $|0\rangle$ (i.e., $\hat{c}_{l\sigma} |0\rangle = 0$ for arbitrary l and σ).

Diagonalizing the above Hamiltonian, we obtain

$$E_{\pm} = \lambda \cos \theta + i\delta_0 \pm i\sqrt{(\sin \theta + \delta_3)^2 + \left(\frac{V}{2}\right)^2}, \quad (8)$$

with $2\delta_0 = \epsilon_{a\uparrow} + \epsilon_{b\uparrow} + \epsilon_{a\downarrow} + \epsilon_{b\downarrow}$ and $2\delta_3 = \epsilon_{a\uparrow} + \epsilon_{b\uparrow} - \epsilon_{a\downarrow} - \epsilon_{b\downarrow}$. Equation (8) elucidates that spin-parity symmetry allows the hybridization term between states with $(N, S^z) = (2, 1)$ and $(N, S^z) = (2, -1)$, which opens the line gap $\text{Im}[E_+(\theta) - E_-(\theta)] > 0$ [see Fig. 2(b)]. In contrast, spin-parity symmetry forbids such hybridization terms for the quadratic Hamiltonian \hat{H}_0 .

The above numerical results support the many-body Hamiltonian $\hat{H}_{(2,1)}(\theta)$ being topologically trivial despite the loop structure due to the topology of the one-body Hamiltonian with $(w, w_s) = (0, 1)$. We can also confirm the robustness of the topology characterized by finite values of $W_{(2,1)}$ [130] (see also Sec. A 2).

Putting the argument in terms of the topological invariants and the above results of the toy model together, we end up with the reduction of the point-gap topology $\mathbb{Z} \times \mathbb{Z} \rightarrow \mathbb{Z}$.

III. POINT-GAP TOPOLOGY IN ONE SPATIAL DIMENSION AND FRAGILITY OF A NON-HERMITIAN SKIN EFFECT

By analyzing an extended Hatano-Nelson chain [see Fig. 3(a)], we elucidate that interactions reduce the point-gap topology in one spatial dimension, as is the case of one synthetic dimension. Remarkably, this reduction phenomenon results in the fragility of a non-Hermitian skin effect against interactions. As in the case of one synthetic dimension, essential ingredients are spin-parity symmetry and two-body terms flipping spins.

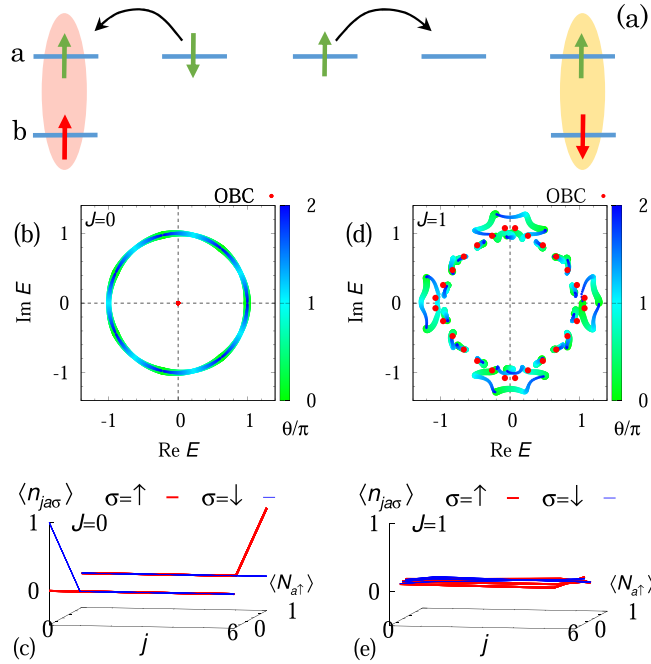


FIG. 3. (a) Sketch of the extended Hatano-Nelson chain. Spectral flows for (b) $J = V = 0$ and (d) $J = V = 1$. Red dots denote the data obtained under the open boundary condition. Expectation values of $\hat{n}_{ja\sigma}$ for (c) $J = V = 0$ and (e) $J = V = 1$ under the open boundary condition. In (c) and (e), $\langle \hat{n}_{ja\sigma} \rangle = {}_R \langle \Phi_n | \hat{n}_{ja\sigma} | \Phi_n \rangle_R$ is plotted against j , and $\langle \hat{N}_{a\uparrow} \rangle = {}_R \langle \Phi_n | \hat{N}_{a\uparrow} | \Phi_n \rangle_R$. Here, $|\Phi_n\rangle_R$ ($n = 0, 1, \dots$) denote the right eigenstates of \hat{H}_{eHN} . Red (blue) lines denote the data for $\sigma = \uparrow$ ($\sigma = \downarrow$). These data are obtained for subsector $(N, P) = (3, -1)$ and parameter set $(L, t) = (7, 1)$.

Let us consider an extended Hatano-Nelson chain [see Fig. 3(a)] whose Hamiltonian reads

$$\hat{H}_{\text{eHN}}(\theta) = \hat{H}_0(\theta) + \hat{H}_{\text{int}}, \quad (9a)$$

$$\hat{H}_0(\theta) = \sum_k \hat{\Psi}_{k\alpha}^\dagger h_{\alpha\beta}(k, \theta) \hat{\Psi}_{k\beta}, \quad (9b)$$

$$\hat{H}_{\text{int}} = \sum_{j=0, L-1} [J(\hat{S}_{ja}^+ \hat{S}_{jb}^- + \text{H.c.}) + iV(\hat{S}_{ja}^+ \hat{S}_{jb}^+ + \text{H.c.})], \quad (9c)$$

with a diagonal matrix $h(k, \theta)$ [$h_{\alpha\beta}(k, \theta) = h_\alpha(k, \theta)\delta_{\alpha\beta}$, $kL/2\pi = 0, 1, \dots, L-1$], whose diagonal elements are

$$h_\alpha(k, \theta) = t\delta_{\alpha, (a, \uparrow)} e^{i(k+\theta/L)} + t\delta_{\alpha, (a, \downarrow)} e^{-i(k+\theta/L)}. \quad (10)$$

Here, we have imposed the twisted boundary condition in order to compute the winding numbers (for more details, see Sec. B 1). The operator $\hat{\Psi}_{k\alpha}$ is the Fourier transformed annihilation operator $\Psi_{k\alpha} := \frac{1}{\sqrt{L}} \sum_{j=0, \dots, L-1} e^{ikj} \Psi_{j\alpha}$, with $\Psi_j^T = (\hat{c}_{ja\uparrow}, \hat{c}_{ja\downarrow}, \hat{c}_{jb\uparrow}, \hat{c}_{jb\downarrow})$. The two-body term \hat{H}_{int} describes the interaction between fermions in orbital a and localized fermions in orbital b . This model also preserves charge $U(1)$ and spin-parity symmetry, meaning that $\hat{H}_{\text{eHN}}(\theta)$ can be block diagonalized with \hat{N} and $\hat{P} = (-1)^{\hat{N}_{a\uparrow} + \hat{N}_{b\uparrow}}$, where $\hat{N}_{l\sigma}$ and \hat{N} are defined as $\hat{N}_{l\sigma} = \sum_j \hat{c}_{jl\sigma}^\dagger \hat{c}_{jl\sigma}$ and $\hat{N} = \sum_{l\sigma} \hat{N}_{l\sigma}$, respectively. The Hamiltonian $\hat{H}_{\text{eHN}}(\theta)$ also commutes with $\hat{n}_{jb} =$

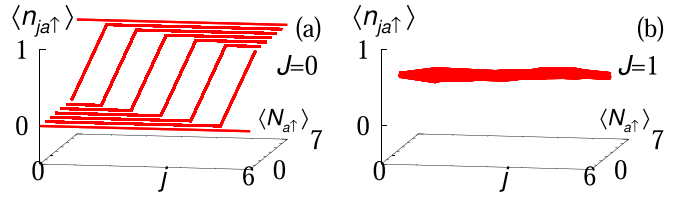


FIG. 4. Expectation values of $\hat{n}_{ja\uparrow}$ for subsector $(N, P) = (9, -1)$ and parameter set $(L, t) = (7, 1)$. In (a) and (b), data for $J = V = 0$ and $J = V = 1$ are plotted, respectively. These figures are plotted in the same way as Figs. 3(c) and 3(e).

$\sum_\sigma \hat{c}_{jb\sigma}^\dagger \hat{c}_{j\sigma}$ for $j = 0, L-1$, and thus, we suppose that orbital b is occupied at both edges ($j = 0, L-1$) by focusing on the corresponding Fock space.

Now, we demonstrate that for $N_a = 1$ (i.e., $N = 3$), a non-Hermitian skin effect observed at the noninteracting level is fragile against the two-body interactions due to trivial topology of the many-body Hamiltonian. Let us start with the noninteracting level. Under the twisted boundary condition, the spectral flow shows a loop structure [see Fig. 3(b)] due to the point-gap topology of the one-body Hamiltonian $h(\theta) := \bigoplus_k h(k, \theta)$ characterized by $(w, w_s) = (0, 1)$ for $\epsilon_{\text{ref}} = 0$. This nontrivial topology of h induces the non-Hermitian skin effect at the noninteracting level. In the presence of the boundaries, all of the eigenvalues E_n ($n = 0, 1, \dots$) become zero, in contrast to the eigenvalues in the absence of the boundaries [see Fig. 3(b)]. In addition, a fermion in the up- (down-) spin state is localized around the right (left) edge under the open boundary condition [see Fig. 3(c)].

However, interactions destroy the above non-Hermitian skin effect due to the trivial topology of the many-body Hamiltonian $W_{(3, -1)} = 0$ for $E_{\text{ref}} = 0$ (for computation of the many-body winding number, see Fig. 6). Because of the trivial topology, we can observe that interactions destroy the loop structure of the spectral flow and open a line gap for $J = V = 1$ [see Fig. 3(d)], which is also confirmed by analysis based on the perturbation theory (see Sec. B 2). This result verifies the reduction of the point-gap topology $\mathbb{Z} \times \mathbb{Z} \rightarrow \mathbb{Z}$ for the subsector with $(N, P) = (3, -1)$. Correspondingly, the interactions destroy the extreme sensitivity of the spectrum to the presence or absence of boundaries [see Fig. 3(d)]. Furthermore, in the presence of interactions, fermions extend to the bulk even under the open boundary condition [see Fig. 3(e)]. This result is also intuitively understood as follows: While the one-body term $\hat{H}_0(\theta)$ localizes the fermions in orbital a and the up- (down-) spin state around the right (left) edge, the two-body interactions \hat{H}_{int} flip their spins at edges, which suppresses the effects of boundaries. The above results indicate that the non-Hermitian skin effect observed at the noninteracting level is fragile against two-body interactions [131]. Our numerical calculations indicate that such fragility of the non-Hermitian skin effect is also observed for the case of many fermions in orbital a (see Fig. 4). More detailed data are provided in Sec. B 3.

IV. SUMMARY AND DISCUSSION

We have analyzed interaction effects on the one-dimensional point-gap topology in both cases of synthetic

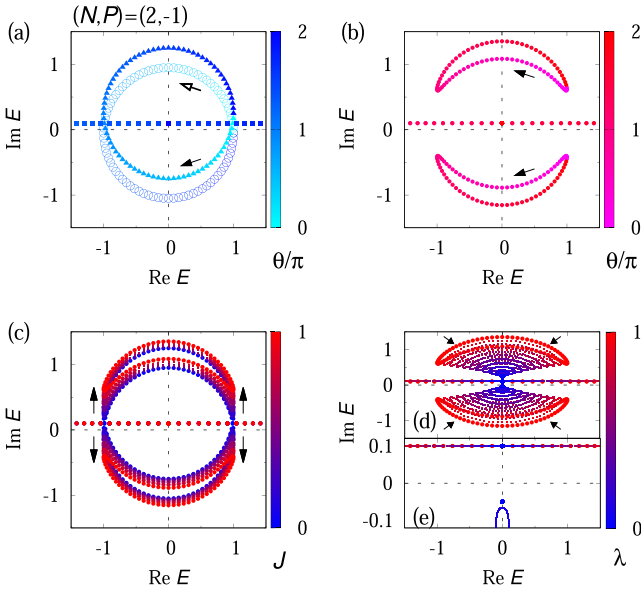


FIG. 5. Spectral flow of the many-body Hamiltonian for the subsector with $(N, P) = (2, -1)$. (a)–(d) are plotted in the same way as Figs. 2(a)–2(d). (e) is a magnified version of the range $-0.12 \leq \text{Re } E \leq 0.12$ and $-0.1 \leq \text{Im } E \leq 0.12$ in (d).

and spatial dimensions. Our analysis has elucidated that the reduction $\mathbb{Z} \times \mathbb{Z} \rightarrow \mathbb{Z}$ occurs for systems of one synthetic dimension with charge $U(1)$ symmetry and spin-parity symmetry. This conclusion was obtained with the argument of topological invariants as well as by explicit analysis of the toy model. Furthermore, we have also analyzed the extended Hatano-Nelson chain, which exhibits striking interaction effects: Interactions reduce the point-gap topology and destroy the non-Hermitian skin effect at the noninteracting level.

We stress that the spin-parity symmetry plays an essential role, which leads to qualitative differences with results of previous works [118,119]. Instead of Eq. (9c), one can introduce Hubbard-type interactions preserving spin $U(1)$ symmetry. This type of interactions does not flip the spins and thus would not destroy the non-Hermitian skin effect as discussed in Refs. [118,119]. Analysis of other types of interactions is left as future work to be addressed. We also note several open questions. Our results indicate that interactions result in the same reduction phenomenon for both cases of synthetic and spatial dimensions whose generality for other symmetry classes remains an open question. In addition, establishing strict one-to-one correspondence between the many-body winding number and skin effect also remains a crucial open question.

The above discoveries shed light on non-Hermitian correlated systems and open up different directions for research on non-Hermitian topological physics. For instance, the above results imply the possibility of similar reduction phenomena for other cases of symmetry and dimensions. As well as the above theoretical open question, experimental observation of the reduction is also a significant issue that needs to be addressed. We believe that cold atoms could be promising candidates where interactions and non-Hermiticity can be tuned in experiments.

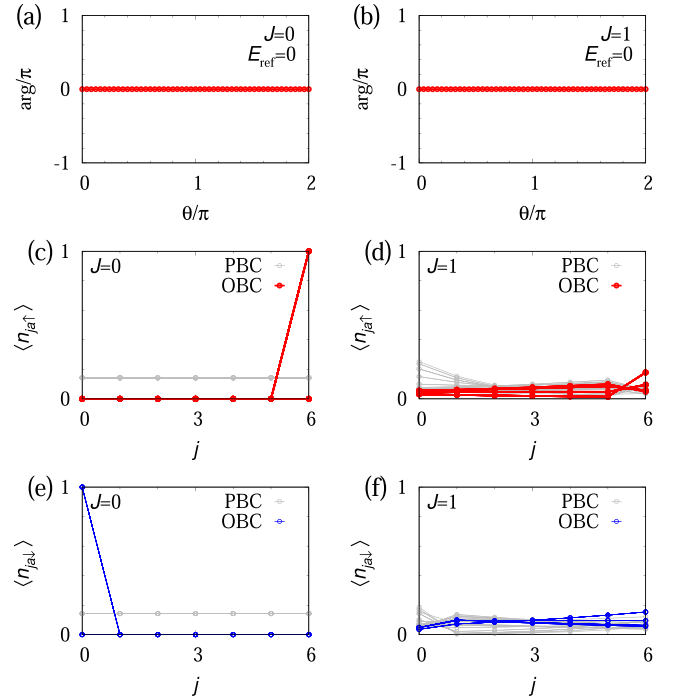


FIG. 6. Data for $(L, t) = (7, 1)$ and subsector $(N, P) = (3, -1)$. (a) and (b) The twist angle θ dependence of $\arg[\prod_n (E_n - E_{\text{ref}})]$ for $E_{\text{ref}} = 0$. Expectation values $\langle \hat{n}_{j\sigma} \rangle = {}_{\text{R}}\langle \Phi_n | \hat{n}_{j\sigma} | \Phi_n \rangle_{\text{R}}$ with (c) and (d) $\sigma = \uparrow$ and (e) and (f) $\sigma = \downarrow$. Here, $|\Phi_n\rangle_{\text{R}}$ ($n = 0, 1, \dots$) denote right eigenstates of \hat{H}_{eHN} . Data obtained under the open boundary condition (the periodic boundary condition) are shown with colored (gray) symbols. (a), (c), and (e) [(b), (d), and (f)] display data for $J = V = 0$ ($J = V = 1$).

ACKNOWLEDGMENTS

This work was supported by MEXT KAKENHI Grant-in-Aid for Transformative Research Areas A “Extreme Universe” Grant No. JP22H05247. This work is also supported by JSPS KAKENHI Grant No. JP21K13850 and also by JST CREST Grant No. JPMJCR19T1, Japan.

APPENDIX A: DETAILS OF A TWO-ORBITAL MODEL

1. Analysis for the subsector with $(N, P) = (2, -1)$

In the main text, we saw that interactions open a line gap for the subsector with $(N, P) = (2, 1)$, which is consistent with the trivial topology $W_{(2,1)} = 0$ for $E_{\text{ref}} = 0$. In this section, we show that a similar behavior is observed for the subsector with $(N, P) = (2, -1)$.

Despite the nontrivial topology of the one-body Hamiltonian, the many-body winding number takes a value of zero ($W_{(2,-1)} = 0$) for $E_{\text{ref}} = 0$, as shown in Fig. 5(a). Correspondingly, the spectrum of the many-body Hamiltonian $\hat{H}_{(2,-1)}$ can smoothly shrink to the points [see Figs. 5(b)–5(d)].

In this subsector, the interaction J is essential for the destruction of the loop structure observed in Fig. 5(a), which can be seen as follows. In the subsector with $(N, P) = (2, -1)$, the Hamiltonian is written as

$$\hat{H}_{(2,-1)} = \hat{H}_{0(2,-1)} + \hat{H}_{\text{int}(2,-1)}, \quad (\text{A1a})$$

$$\hat{H}_{0(2,-1)} = \text{diag}(\lambda e^{i\theta} + i\epsilon_{a\uparrow} + i\epsilon_{b\downarrow}, \lambda e^{-i\theta} + i\epsilon_{a\downarrow} + i\epsilon_{b\uparrow} \\ \times 2\lambda \cos \theta + i\epsilon_{a\uparrow} + i\epsilon_{a\downarrow}, i\epsilon_{b\uparrow} + i\epsilon_{b\downarrow}), \quad (\text{A1b})$$

$$\hat{H}_{\text{int}(2,-1)} = \frac{iJ}{2} \begin{pmatrix} 0 & 1 & 0 & 0 \\ 1 & 0 & 0 & 0 \\ 0 & 0 & 0 & 0 \\ 0 & 0 & 0 & 0 \end{pmatrix}, \quad (\text{A1c})$$

with $\text{diag}(\dots)$ denoting a diagonal matrix. Here, we have chosen the following basis vectors spanning the subsector of the Fock space:

$$(\hat{c}_{a\uparrow}^\dagger \hat{c}_{b\downarrow}^\dagger |0\rangle, \hat{c}_{a\downarrow}^\dagger \hat{c}_{b\uparrow}^\dagger |0\rangle, \hat{c}_{a\uparrow}^\dagger \hat{c}_{a\downarrow}^\dagger |0\rangle, \hat{c}_{b\uparrow}^\dagger \hat{c}_{b\downarrow}^\dagger |0\rangle). \quad (\text{A2})$$

Diagonalizing the Hamiltonian, we obtain

$$E_{\pm} = \lambda \cos \theta + i\delta'_0 \pm i\sqrt{(\sin \theta + \delta'_3)^2 + \left(\frac{J}{2}\right)^2}, \quad (\text{A3})$$

$$E' = 2\lambda \cos \theta + i\epsilon_{a\uparrow} + i\epsilon_{a\downarrow}, \quad (\text{A4})$$

$$E'' = i\epsilon_{b\uparrow} + i\epsilon_{b\downarrow}, \quad (\text{A5})$$

with $2\delta'_0 = \epsilon_{a\uparrow} + \epsilon_{b\downarrow} + \epsilon_{a\downarrow} + \epsilon_{b\uparrow}$ and $2\delta'_3 = \epsilon_{a\uparrow} + \epsilon_{b\downarrow} - (\epsilon_{a\downarrow} + \epsilon_{b\uparrow})$. The above results elucidate that the spin-parity symmetry allows the two-body interaction which splits the loop structure observed in Fig. 5(a).

2. Robustness of the topology characterized by $W_{(2,1)} = 2$

Let us analyze a toy model in order to demonstrate the robustness of the topology characterized by $W_{(2,1)} = 2$. Specifically, we consider \hat{H} specified by

$$h_{\alpha}(\theta) = \lambda e^{i\theta} (\delta_{\alpha,(a,\uparrow)} + \delta_{\alpha,(a,\downarrow)}) + i\epsilon_{l\sigma} \delta_{\alpha,(l,\sigma)} \quad (\text{A6})$$

and the interaction term [Eq. (7)]. Then, we have

$$\hat{H}_{(2,1)} = \begin{pmatrix} \lambda e^{i\theta} + i\epsilon_{a\uparrow} + i\epsilon_{b\uparrow} & & & \\ & \frac{iV}{2} & & \\ & & \lambda e^{i\theta} + i\epsilon_{a\downarrow} + i\epsilon_{b\downarrow} & \\ & & & \frac{iV}{2} \end{pmatrix}$$

for the subsector with $(N, P) = (2, 1)$ [see also arguments above Eq. (8)]. Diagonalizing the above Hamiltonian, we obtain

$$E_{\pm} = \lambda e^{i\theta} + i\delta_0 \pm i\sqrt{(\delta_3)^2 + \left(\frac{V}{2}\right)^2}, \quad (\text{A7})$$

where δ_0 and δ_3 are defined just below Eq. (8). This result demonstrates that the topology characterized by $W_{(2,1)} = 2$ is robust against interactions. Let us choose the parameters as $\delta_0 = \delta_3 = 0$. In this case, Eqs. (5) and (A7) indicate that the topology is characterized by $W_{(2,1)} = 2$ for $E_{\text{ref}} = 0$ in the absence of the interactions. Equation (A7) also indicates that this nontrivial topology is maintained for finite values of V .

APPENDIX B: DETAILS OF THE EXTENDED HATANO-NELSON CHAIN

1. Hamiltonian under the twisted boundary condition

We provide the explicit form of the extended Hatano-Nelson chain under the twisted boundary condition. The

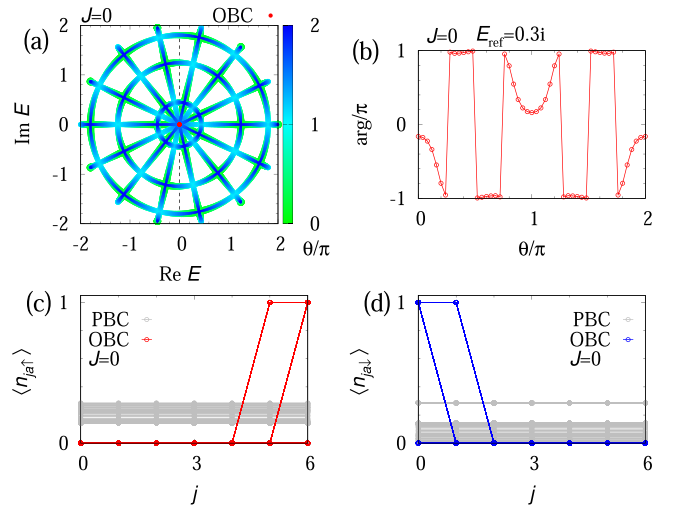


FIG. 7. Numerical data for $J = V = 0$ and subsector $(N, P) = (4, 1)$. (a) Spectral flow of the many-body Hamiltonian. (b) The twist angle θ dependence of $\arg[\prod_n (E_n - E_{\text{ref}})]$ for $E_{\text{ref}} = 0.3i$. Expectation values $\langle \hat{n}_{j\sigma} \rangle = {}_{\text{R}}\langle \Phi_n | \hat{n}_{j\sigma} | \Phi_n \rangle_{\text{R}}$ with (c) and (d) $\sigma = \downarrow$ and (e) and (f) $\sigma = \uparrow$. Here, $|\Phi_n\rangle_{\text{R}} (n = 0, 1, \dots)$ denote right eigenstates of $\hat{H}_{\text{eHN}}(\theta = 0)$. Data obtained under the open boundary condition (the periodic boundary condition) are shown with colored (gray) symbols. These data are obtained for parameter set $(L, t) = (7, 1)$.

Hamiltonian reads

$$\hat{H}_{\text{eHN}} = \hat{H}_0(\theta) + \hat{H}_{\text{int}}, \quad (\text{B1a})$$

$$\hat{H}_0(\theta) = t \left[e^{i\theta} \hat{c}_{0a\uparrow}^\dagger \hat{c}_{L-1a\uparrow} + \sum_{j=0}^{L-2} \hat{c}_{j+1a\uparrow}^\dagger \hat{c}_{ja\uparrow} \right] \\ + t \left[e^{-i\theta} \hat{c}_{L-1a\downarrow}^\dagger \hat{c}_{0a\downarrow} + \sum_{j=1}^{L-1} \hat{c}_{j-1a\downarrow}^\dagger \hat{c}_{ja\downarrow} \right], \quad (\text{B1b})$$

$$\hat{H}_{\text{int}}(\theta) = \sum_{j=0, L-1} \left[\frac{J}{2} (\hat{S}_{ja}^+ \hat{S}_{jb}^- + \hat{S}_{ja}^- \hat{S}_{jb}^+) \right. \\ \left. + iV (\hat{S}_{ja}^+ \hat{S}_{jb}^+ + \hat{S}_{ja}^- \hat{S}_{jb}^-) \right]. \quad (\text{B1c})$$

Under a gauge transformation $\hat{c}_{j\sigma} \rightarrow e^{-i\frac{\theta}{L}j} \hat{c}_{j\sigma}$, the one-body term is written as

$$\hat{H}_0(\theta) = \sum_{j=0}^{L-1} [t e^{i\theta/L} \hat{c}_{j+1a\uparrow}^\dagger \hat{c}_{ja\uparrow} + t e^{-i\theta/L} \hat{c}_{j-1a\downarrow}^\dagger \hat{c}_{ja\downarrow}], \quad (\text{B2})$$

with $\hat{c}_{La\uparrow}^\dagger := \hat{c}_{0a\uparrow}^\dagger$ and $\hat{c}_{-1a\downarrow}^\dagger := \hat{c}_{L-1a\downarrow}^\dagger$.

Applying the Fourier transformation to the above Hamiltonian yields Eq. (10). We note that under the open boundary condition, hopping terms between sites $j = 0$ and $j = L - 1$ [i.e., the first and third terms of Eq. (B1b)] become zero.

In the presence of charge $U(1)$ symmetry and spin-parity symmetry, the one-body Hamiltonian is characterized by w and w_s [Eqs. (3) and (4)] with $h(\theta) := \oplus_k h(k, \theta)$. The topology of the many-body Hamiltonian for a given subsector with (N, P) is characterized by the many-body winding number [Eq. (5)] with $\hat{H}_{(N,P)} := \hat{H}_{\text{eHN}(N,P)}$. Here, $\hat{H}_{\text{eHN}(N,P)}$ denotes

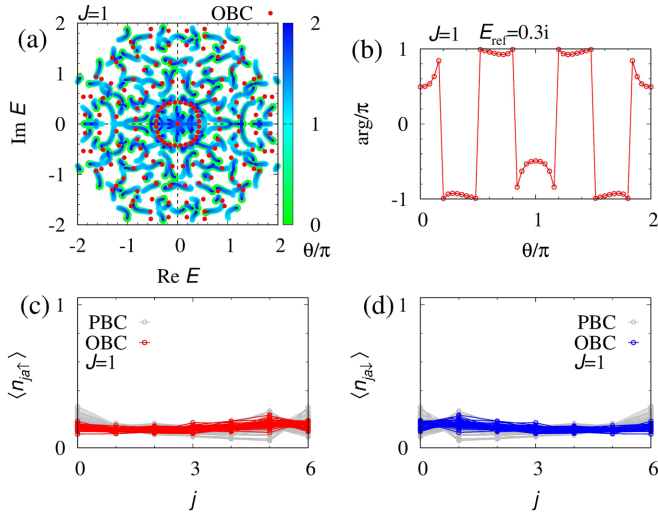


FIG. 8. Numerical data for $J = V = 1$ and subsector $(N, P) = (4, 1)$. These figures are plotted in the same way as Figs. 7(a)–7(d).

the many-body Hamiltonian of the extended Hatano-Nelson model for the given subsector with (N, P) .

2. Analysis based on the perturbation theory

Based on the perturbation theory, we confirm that interactions open a line gap as shown in Fig. 3(d). As mentioned in the main text, we suppose that orbital b is occupied at both edges ($j = 0, L - 1$).

Suppose that interactions are sufficiently weak. In the subsector with $(N, P) = (3, -1)$, the noninteracting Hamiltonian $\hat{H}_0(\theta)$ is written as

$$\hat{H}_{0(3,-1)} = t\omega^n \begin{pmatrix} e^{i\frac{\theta}{L}} & 0 & 0 & 0 \\ 0 & e^{i\frac{\theta}{L}} & 0 & 0 \\ 0 & 0 & e^{-i\frac{\theta}{L}} & 0 \\ 0 & 0 & 0 & e^{-i\frac{\theta}{L}} \end{pmatrix}, \quad (\text{B3})$$

with $\omega = e^{\frac{2\pi i}{L}}$ and the basis

$$(|n \uparrow; \uparrow \uparrow\rangle, |n \uparrow; \downarrow \downarrow\rangle, |n \downarrow; \uparrow \downarrow\rangle, |n \downarrow; \downarrow \uparrow\rangle) \quad (\text{B4})$$

for given n ($n = 0, 1, 2, \dots, L - 1$). Here, $|n\sigma; \sigma'\sigma''\rangle$ is defined as $|n\sigma; \sigma'\sigma''\rangle := \tilde{d}_{n\sigma} \hat{c}_{0b\sigma'}^\dagger \hat{c}_{L-1b\sigma''}^\dagger |0\rangle$, with $\tilde{d}_{n\uparrow} := \sum_j \hat{c}_{ja\uparrow}^\dagger R_{jn}$ and $\tilde{d}_{n\downarrow} := \sum_j \hat{c}_{ja\downarrow}^\dagger L_{jn}^*$. Matrices R and L^\dagger ($R_{jn} := \frac{1}{\sqrt{L}} \omega^{-nj}$ and $L_{nj}^\dagger := \frac{1}{\sqrt{L}} \omega^{nj}$) diagonalize the matrix h ($h_{ij} = t\delta_{i,j+1}$),

$$L^\dagger h R = t \text{diag}(1, \omega, \omega^2, \dots, \omega^{L-1}), \quad (\text{B5})$$

which corresponds to the kinetic term of fermions in orbital a and the up-spin state for $\theta = 0$ [see Eq. (B1b) and Fig. 3(a)]. Here $\text{diag}(\dots)$ describes a diagonal matrix. Introducing the operators $\hat{d}_{n\uparrow} := \sum_j \hat{c}_{ja\uparrow} (L^\dagger)_{nj}$ and $\hat{d}_{n\downarrow} := \sum_j \hat{c}_{ja\downarrow} (R^T)_{nj}$, we have anticommutation relations

$$\{\hat{d}_{n\sigma}, \tilde{d}_{m\sigma'}\} = \delta_{nm} \delta_{\sigma\sigma'} \quad (\text{B6})$$

for $n, m = 0, 1, 2, \dots, L - 1$ and $\sigma, \sigma' = \uparrow, \downarrow$, which can be seen by noting the relations $\sum_j L_{nj}^\dagger R_{jm} = \delta_{nm}$ and

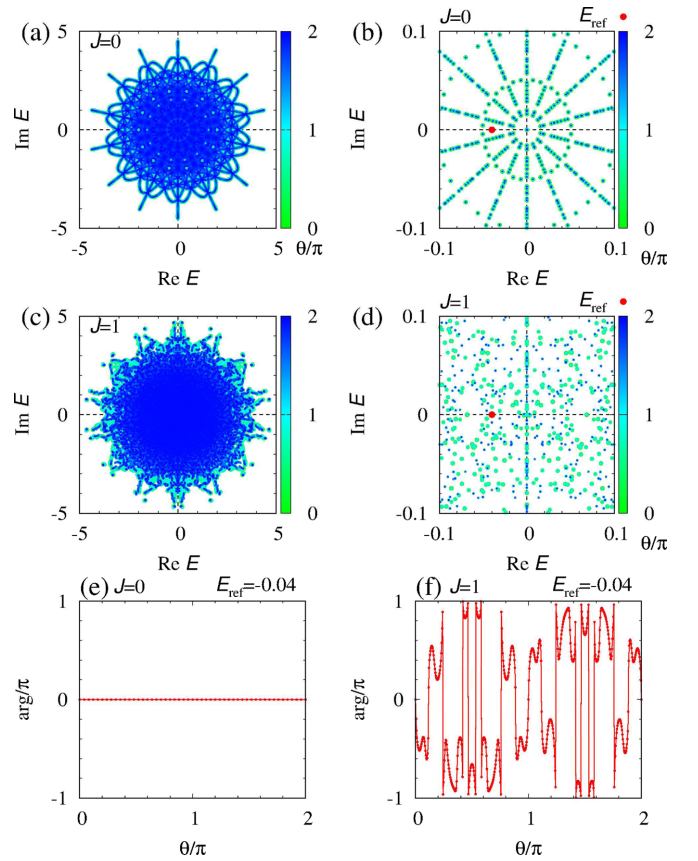


FIG. 9. Data for $(L, t) = (7, 1)$ and subsector $(N, P) = (9, -1)$. [(c) and (d)]: Spectral flow for (a) and (b) $J = V = 0$ and (c) and (d) $J = V = 1$. (b) and (d) are magnified versions of the ranges $-0.1 \leq \text{Im} E \leq 0.1$ and $-0.1 \leq \text{Re} E \leq 0.1$ in (a) and (c), respectively. The twist angle θ dependence of $\arg[\prod_n (E_n - E_{\text{ref}})]$ for $E_{\text{ref}} = -0.04$ and (e) $J = V = 0$ and (f) $J = V = 1$.

$\{\hat{c}_{i\sigma}, \hat{c}_{j'\sigma'}^\dagger\} = \delta_{ij} \delta_{\sigma\sigma'}$. We note that $(\tilde{d}_{n\sigma}^\dagger)^\dagger = \hat{d}_{n\sigma}$ holds due to the relation $R_{jn}^* = L_{nj}^\dagger$.

Now, let us compute energy eigenvalues at the first order of the interactions. First, we note the following relations:

$$\begin{aligned} \hat{S}_{ja}^+ |m \downarrow; \sigma\sigma'\rangle &= \sum_i \hat{S}_{ja}^+ L_{im}^* \hat{c}_{ia\downarrow}^\dagger \hat{c}_{0b\sigma}^\dagger \hat{c}_{L-1b\sigma'}^\dagger |0\rangle \\ &= L_{jm}^* \hat{c}_{ja\uparrow}^\dagger \hat{c}_{0b\sigma}^\dagger \hat{c}_{L-1b\sigma'}^\dagger |0\rangle \\ &= \sum_n L_{jm}^* (L^\dagger)_{nj} \tilde{d}_{n\uparrow} \hat{c}_{0b\sigma}^\dagger \hat{c}_{L-1b\sigma'}^\dagger |0\rangle \\ &= \frac{1}{L} \sum_n \omega^{(n+m)j} |n \uparrow; \sigma\sigma'\rangle, \end{aligned} \quad (\text{B7})$$

$$\begin{aligned} \hat{S}_{ja}^- |m \uparrow; \sigma\sigma'\rangle &= \sum_i \hat{S}_{ja}^- R_{im} \hat{c}_{ia\uparrow}^\dagger \hat{c}_{0b\sigma}^\dagger \hat{c}_{L-1b\sigma'}^\dagger |0\rangle \\ &= R_{jm} \hat{c}_{ja\downarrow}^\dagger \hat{c}_{0b\sigma}^\dagger \hat{c}_{L-1b\sigma'}^\dagger |0\rangle \\ &= \sum_n R_{jm} (R^T)_{nj} \tilde{d}_{n\downarrow} \hat{c}_{0b\sigma}^\dagger \hat{c}_{L-1b\sigma'}^\dagger |0\rangle \\ &= \frac{1}{L} \sum_n \omega^{-(n+m)j} |n \downarrow; \sigma\sigma'\rangle. \end{aligned} \quad (\text{B8})$$

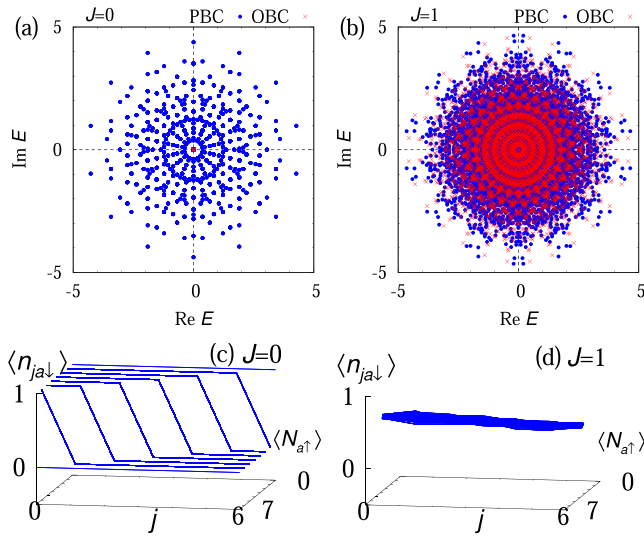


FIG. 10. (a) and (b) Spectrum of the many-body Hamiltonian for $J = V = 0$ and $J = V = 1$, respectively. Blue (red) symbols denote data obtained under the periodic (open) boundary condition. (c) and (d) Expectation values $\langle \hat{n}_{ja\downarrow} \rangle = {}_R \langle \Phi_n | \hat{n}_{ja\downarrow} | \Phi_n \rangle_R$ against j and $\langle \hat{N}_{a\uparrow} \rangle = {}_R \langle \Phi_n | \hat{N}_{a\uparrow} | \Phi_n \rangle_R$ for $J = V = 0$ and $J = V = 1$, respectively. These data are obtained for $(L, t) = (7, 1)$ and subsector $(N, P) = (9, -1)$.

Here, we have used the relations $\sum_n R_{jn} L_{ni}^\dagger = \delta_{ij}$, $\hat{c}_{ia\uparrow}^\dagger = \sum_n L_{ni}^\dagger \hat{d}_{n\uparrow}^\dagger$, and $\hat{c}_{ia\downarrow}^\dagger = \sum_n R_{ni}^\dagger \hat{d}_{n\downarrow}^\dagger$.

Thus, at the first order, the Hamiltonian is written as $\hat{H}_{\text{eHN}(3,1)} = \hat{H}_{0(3,1)} + \hat{H}_{\text{int}(3,1)}$ with $\hat{H}_{0(3,1)}$ in Eq. (B3) and

$$\hat{H}_{\text{int}(3,-1)} = \frac{V}{L} \begin{pmatrix} 0 & 0 & \omega^{-2n} & 1 \\ 0 & 0 & 0 & 0 \\ \omega^{2n} & 0 & 0 & 0 \\ 1 & 0 & 0 & 0 \end{pmatrix} + \frac{iJ}{L} \begin{pmatrix} 0 & 0 & 0 & 0 \\ 0 & 0 & 1 & \omega^{-2n} \\ 0 & 1 & 0 & 0 \\ 0 & \omega^{2n} & 0 & 0 \end{pmatrix} \quad (\text{B9})$$

for the basis defined in Eq. (B4).

The eigenvalues of $\hat{H}_{\text{eHN}(3,1)}$ are written as

$$E_{p,\pm} = t\omega^n \left(\cos\left(\frac{\theta}{L}\right) \pm \sqrt{C_p^2 - \sin^2\left(\frac{\theta}{L}\right)} \right), \quad (\text{B10a})$$

$$E_{m,\pm} = t\omega^n \left(\cos\left(\frac{\theta}{L}\right) \pm \sqrt{C_m^2 - \sin^2\left(\frac{\theta}{L}\right)} \right), \quad (\text{B10b})$$

with

$$C_p^2 = \frac{1}{(t\omega^n L)^2} [(V^2 - J^2) + \sqrt{V^4 + J^4 - 2V^2 J^2 \text{Re}[\omega^{4n}]}], \quad (\text{B10c})$$

$$C_m^2 = \frac{1}{(t\omega^n L)^2} [(V^2 - J^2) - \sqrt{V^4 + J^4 - 2V^2 J^2 \text{Re}[\omega^{4n}]}]. \quad (\text{B10d})$$

As well as by directly diagonalizing the matrix, the eigenvalues are obtained by taking the square of the matrices (see below). These results indicate that interactions lift the fourfold degeneracy observed for $\theta = 0$. Specifically, the imaginary parts of C_p and C_m lift the degeneracy. To see this, first, let us suppose that the imaginary parts are zero ($\text{Im}C_p = \text{Im}C_m = 0$). Then, Eq. (B10a) indicates that exceptional points emerge at certain θ [i.e., $C_p^2 \geq 0$ holds, and $C_p^2 - \sin^2(\theta/L) = 0$ can be satisfied]. On the other hand, the finite imaginary parts lift the degeneracy at $\theta = 0$ without inducing exceptional points [i.e., $C_p^2 - \sin^2(\theta/L) \neq 0$ for $0 \leq \theta < 2\pi$].

Equations (B10c) and (B10d) indicate that the imaginary parts of C_p and C_m can be finite for a proper choice of n, J , and V . Therefore, the above result for the first-order perturbation theory indicates that interactions open a line gap.

We show that eigenvalues (B10) can be obtained by taking the squares of the matrices. Consider the following matrix:

$$\tilde{H} = (x\sigma_0\tau_0 + y\sigma_0\tau_3 + a\sigma_1\tau_1 + b\sigma_2\tau_2 + c\sigma_0\tau_1 + d\sigma_3\tau_1 + f\sigma_0\tau_2 + g\sigma_3\tau_2), \quad (\text{B11})$$

with complex numbers x, y, a, b, c, d, f , and g . Here, σ_0 and τ_0 denote the 2×2 identity matrix. Pauli matrices are denoted by σ_s and τ_s ($s = 1, 2, 3$). Matrices $\sigma_\mu \tau_\nu$ ($\mu, \nu = 0, 1, 2, 3$) denote 4×4 matrices. For instance, $\sigma_1 \tau_2$ is written as

$$\sigma_1 \tau_2 = \begin{pmatrix} 0 & 0 & 0 & -i \\ 0 & 0 & -i & 0 \\ 0 & i & 0 & 0 \\ i & 0 & 0 & 0 \end{pmatrix}. \quad (\text{B12})$$

For the parameter set

$$\begin{pmatrix} x \\ y \\ a \\ b \\ c \\ d \\ f \\ g \end{pmatrix} = \frac{1}{2L} \begin{pmatrix} 2Lt\omega^n \cos\frac{\theta}{L} \\ 2iLt\omega^n \sin\frac{\theta}{L} \\ V + iJ \\ -V + iJ \\ (V + iJ)\text{Re}(\omega^{2n}) \\ (V - iJ)\text{Re}(\omega^{2n}) \\ (V + iJ)\text{Im}(\omega^{2n}) \\ (V - iJ)\text{Im}(\omega^{2n}) \end{pmatrix}, \quad (\text{B13})$$

\tilde{H} is reduced to the matrix $\hat{H}_{\text{eHN}(3,-1)}$.

Taking the square of this matrix yields

$$\begin{aligned} & (\tilde{H} - x\sigma_0\tau_0)^2 - (y^2 + a^2 + b^2 + c^2 + d^2 + f^2 + g^2) \\ & = -2ab\sigma_3\tau_3 + 2(cd + fg)\sigma_3\tau_0 + 2ac\sigma_1\tau_0 + 2ag\sigma_2\tau_3 \\ & \quad + 2bd\sigma_1\tau_3 + 2bf\sigma_2\tau_0. \end{aligned} \quad (\text{B14})$$

Thus, we have

$$\begin{aligned}
& [(\tilde{H} - x\sigma_0\tau_0)^2 - (y^2 + a^2 + b^2 + c^2 + d^2 + f^2 + g^2)^2] \\
&= \{[-2ab\sigma_3\tau_3 + 2(cd + fg)\sigma_3\tau_0] + (2ac\sigma_1\tau_0 + 2bd\sigma_1\tau_3) + (2ag\sigma_2\tau_3 + 2bf\sigma_2\tau_0)\}^2 \\
&= \{-2ab\sigma_3\tau_3 + 2(cd + fg)\sigma_3\tau_0\}^2 + (2ac\sigma_1\tau_0 + 2bd\sigma_1\tau_3)^2(2ag\sigma_2\tau_3 + 2bf\sigma_2\tau_0)^2 \\
&= 4\{(ab)^2 + (cd + fg)^2 + (ac)^2 + (bd)^2 + (ag)^2 + (bf)^2\} - 8ab(cd + fg)\sigma_0\tau_3 + 8acbd\sigma_0\tau_3 + 8agbf\sigma_0\tau_3 \\
&= 4\{(ab)^2 + (cd + fg)^2 + (ac)^2 + (bd)^2 + (ag)^2 + (bf)^2\}. \tag{B15}
\end{aligned}$$

Therefore, the eigenvalues are written as

$$E'_{p\pm} = x \pm \sqrt{y^2 + C_p'^2}, \tag{B16}$$

$$E'_{m\pm} = x \pm \sqrt{y^2 + C_m'^2}, \tag{B17}$$

with

$$C_p'^2 = a^2 + b^2 + c^2 + d^2 + f^2 + g^2 + 2\sqrt{(ab)^2 + (cd + fg)^2 + (ac)^2 + (bd)^2 + (ag)^2 + (bf)^2}, \tag{B18}$$

$$C_m'^2 = a^2 + b^2 + c^2 + d^2 + f^2 + g^2 - 2\sqrt{(ab)^2 + (cd + fg)^2 + (ac)^2 + (bd)^2 + (ag)^2 + (bf)^2}. \tag{B19}$$

Thus, choosing the parameters in Eq. (B13), we obtain Eq. (B10).

3. Numerical results

In the main text, we briefly discussed the extended Hatano-Nelson chain. Here, let us numerically analyze this system in detail. First, we focus on the subsector with $(N, P) = (3, -1)$ (see Fig. 6). Although the topology of the one-body Hamiltonian is nontrivial [i.e., $(w, w_s) = (0, 1)$ for $\epsilon_{\text{ref}} = 0$], the many-body Hamiltonian is topologically trivial (i.e., $W_{(3,-1)} = 0$ for $E_{\text{ref}} = 0$), as shown in Figs. 6(a) and 6(b). This fact results in the fragility of the non-Hermitian skin effect against interactions. Namely, although the fermion with the up- (down-) spin state is localized at the right (left) edge due to the non-Hermitian skin effect in the noninteracting case [see Figs. 6(c) and 6(e)], such a localization cannot be observed in the presence of the interactions [see Figs. 6(d) and 6(f)]. Correspondingly, the extreme sensitivity of the energy spectrum to the boundary condition is not observed for $J = V = 1$ [see Figs. 3(b) and 3(d)].

This fragility of the non-Hermitian skin effect is intuitively understood as follows: the interactions flip the spin

of fermions in orbital a , which suppresses the effects of the boundaries.

Now, let us focus on the subsector with $(N, P) = (4, 1)$ (see Figs. 7 and 8). Figures 7(a) and 7(b) indicate the topology of the many-body Hamiltonian is trivial. However, due to the topology of the one-body Hamiltonian, we can observe the extreme sensitivity of the spectrum and expectation values $\langle \hat{n}_{j\alpha\sigma} \rangle$ to the presence or absence of the boundaries [see Figs. 7(c) and 7(d)]. As is the case for $(N, P) = (3, -1)$, such extreme sensitivity is fragile against interactions (see Fig. 8).

Finally, we discuss the case for $(N, P) = (9, -1)$, where orbital a is half filled. Figure 9 indicates that the many-body Hamiltonian is topologically trivial, which results in the fragility of the non-Hermitian skin effect at the noninteracting level as discussed above. Namely, while the topology of the one-body Hamiltonian induces the extreme sensitivity of the energy spectrum and the expectation values $\langle \hat{n}_{ja\downarrow} \rangle$ to the boundary conditions, such extreme sensitivity is not observed in the interacting case (see Fig. 10).

-
- [1] D. J. Thouless, M. Kohmoto, M. P. Nightingale, and M. den Nijs, *Phys. Rev. Lett.* **49**, 405 (1982).
[2] Y. Hatsugai, *Phys. Rev. Lett.* **71**, 3697 (1993).
[3] A. Y. Kitaev, *Phys. Usp.* **44**, 131 (2001).
[4] C. L. Kane and E. J. Mele, *Phys. Rev. Lett.* **95**, 146802 (2005).
[5] C. L. Kane and E. J. Mele, *Phys. Rev. Lett.* **95**, 226801 (2005).
[6] X.-L. Qi, T. L. Hughes, and S.-C. Zhang, *Phys. Rev. B* **78**, 195424 (2008).
[7] M. Z. Hasan and C. L. Kane, *Rev. Mod. Phys.* **82**, 3045 (2010).
[8] X.-L. Qi and S.-C. Zhang, *Rev. Mod. Phys.* **83**, 1057 (2011).
[9] M. Sato and S. Fujimoto, *J. Phys. Soc. Jpn.* **85**, 072001 (2016).
[10] D. C. Tsui, H. L. Stormer, and A. C. Gossard, *Phys. Rev. Lett.* **48**, 1559 (1982).
[11] R. B. Laughlin, *Phys. Rev. Lett.* **50**, 1395 (1983).
[12] J. K. Jain, *Phys. Rev. Lett.* **63**, 199 (1989).
[13] X.-G. Wen, *Quantum Field Theory of Many-Body Systems: From the Origin of Sound to an Origin of Light and Electrons* (Oxford University Press, Oxford, 2004).
[14] M. A. Levin and X.-G. Wen, *Phys. Rev. B* **71**, 045110 (2005).
[15] A. Kitaev, *Ann. Phys. (NY)* **303**, 2 (2003).
[16] A. Kitaev, *Ann. Phys. (NY)* **321**, 2 (2006).
[17] L. Fidkowski and A. Kitaev, *Phys. Rev. B* **81**, 134509 (2010).
[18] A. M. Turner, F. Pollmann, and E. Berg, *Phys. Rev. B* **83**, 075102 (2011).
[19] L. Fidkowski and A. Kitaev, *Phys. Rev. B* **83**, 075103 (2011).
[20] H. Yao and S. Ryu, *Phys. Rev. B* **88**, 064507 (2013).
[21] S. Ryu and S.-C. Zhang, *Phys. Rev. B* **85**, 245132 (2012).
[22] X.-L. Qi, *New J. Phys.* **15**, 065002 (2013).

- [23] Y.-M. Lu and A. Vishwanath, *Phys. Rev. B* **93**, 155121 (2016).
- [24] M. Levin, *Phys. Rev. X* **3**, 021009 (2013).
- [25] H. Isobe and L. Fu, *Phys. Rev. B* **92**, 081304 (2015).
- [26] T. Yoshida, A. Daido, Y. Yanase, and N. Kawakami, *Phys. Rev. Lett.* **118**, 147001 (2017).
- [27] L. Fidkowski, X. Chen, and A. Vishwanath, *Phys. Rev. X* **3**, 041016 (2013).
- [28] C. Wang, A. C. Potter, and T. Senthil, *Science* **343**, 629 (2014).
- [29] M. A. Metlitski, L. Fidkowski, X. Chen, and A. Vishwanath, [arXiv:1406.3032](https://arxiv.org/abs/1406.3032).
- [30] C. Wang and T. Senthil, *Phys. Rev. B* **89**, 195124 (2014).
- [31] Y.-Z. You and C. Xu, *Phys. Rev. B* **90**, 245120 (2014).
- [32] T. Morimoto, A. Furusaki, and C. Mudry, *Phys. Rev. B* **92**, 125104 (2015).
- [33] C.-M. Jian and C. Xu, *Phys. Rev. X* **8**, 041030 (2018).
- [34] O. Boada, A. Celi, J. I. Latorre, and M. Lewenstein, *Phys. Rev. Lett.* **108**, 133001 (2012).
- [35] A. Celi, P. Massignan, J. Ruseckas, N. Goldman, I. B. Spielman, G. Juzeliūnas, and M. Lewenstein, *Phys. Rev. Lett.* **112**, 043001 (2014).
- [36] S. Nakajima, T. Tomita, S. Taie, T. Ichinose, H. Ozawa, L. Wang, M. Troyer, and Y. Takahashi, *Nat. Phys.* **12**, 296 (2016).
- [37] M. Lohse, C. Schweizer, O. Zilberberg, M. Aidelsburger, and I. Bloch, *Nat. Phys.* **12**, 350 (2016).
- [38] N. Hatano and D. R. Nelson, *Phys. Rev. Lett.* **77**, 570 (1996).
- [39] C. M. Bender and S. Boettcher, *Phys. Rev. Lett.* **80**, 5243 (1998).
- [40] Y. C. Hu and T. L. Hughes, *Phys. Rev. B* **84**, 153101 (2011).
- [41] K. Esaki, M. Sato, K. Hasebe, and M. Kohmoto, *Phys. Rev. B* **84**, 205128 (2011).
- [42] E. J. Bergholtz, J. C. Budich, and F. K. Kunst, *Rev. Mod. Phys.* **93**, 015005 (2021).
- [43] Y. Ashida, Z. Gong, and M. Ueda, *Adv. Phys.* **69**, 249 (2020).
- [44] V. M. Martínez Alvarez, J. E. Barrios Vargas, and L. E. F. Foa Torres, *Phys. Rev. B* **97**, 121401(R) (2018).
- [45] F. K. Kunst, E. Edvardsson, J. C. Budich, and E. J. Bergholtz, *Phys. Rev. Lett.* **121**, 026808 (2018).
- [46] S. Yao and Z. Wang, *Phys. Rev. Lett.* **121**, 086803 (2018).
- [47] S. Yao, F. Song, and Z. Wang, *Phys. Rev. Lett.* **121**, 136802 (2018).
- [48] K. Yokomizo and S. Murakami, *Phys. Rev. Lett.* **123**, 066404 (2019).
- [49] E. Edvardsson, F. K. Kunst, and E. J. Bergholtz, *Phys. Rev. B* **99**, 081302(R) (2019).
- [50] Z. Gong, Y. Ashida, K. Kawabata, K. Takasan, S. Higashikawa, and M. Ueda, *Phys. Rev. X* **8**, 031079 (2018).
- [51] J. Carlström and E. J. Bergholtz, *Phys. Rev. A* **98**, 042114 (2018).
- [52] J. Carlström, M. Stålhammar, J. C. Budich, and E. J. Bergholtz, *Phys. Rev. B* **99**, 161115(R) (2019).
- [53] H. Zhou and J. Y. Lee, *Phys. Rev. B* **99**, 235112 (2019).
- [54] K. Kawabata, K. Shiozaki, M. Ueda, and M. Sato, *Phys. Rev. X* **9**, 041015 (2019).
- [55] N. Okuma and M. Sato, *Phys. Rev. Lett.* **123**, 097701 (2019).
- [56] T. Katō, *Perturbation Theory for Linear Operators*, Vol. 132 (Springer, Berlin, 1966), <https://doi.org/10.1007/978-3-642-66282-9>.
- [57] I. Rotter, *J. Phys. A* **42**, 153001 (2009).
- [58] M. V. Berry, *Czech. J. Phys.* **54**, 1039 (2004).
- [59] W. D. Heiss, *J. Phys. A* **45**, 444016 (2012).
- [60] H. Shen, B. Zhen, and L. Fu, *Phys. Rev. Lett.* **120**, 146402 (2018).
- [61] J. C. Budich, J. Carlström, F. K. Kunst, and E. J. Bergholtz, *Phys. Rev. B* **99**, 041406(R) (2019).
- [62] T. Yoshida, R. Peters, N. Kawakami, and Y. Hatsugai, *Phys. Rev. B* **99**, 121101(R) (2019).
- [63] R. Okugawa and T. Yokoyama, *Phys. Rev. B* **99**, 041202(R) (2019).
- [64] H. Zhou, J. Y. Lee, S. Liu, and B. Zhen, *Optica* **6**, 190 (2019).
- [65] K. Kawabata, T. Bessho, and M. Sato, *Phys. Rev. Lett.* **123**, 066405 (2019).
- [66] K. Kimura, T. Yoshida, and N. Kawakami, *Phys. Rev. B* **100**, 115124 (2019).
- [67] T. Yoshida, R. Peters, N. Kawakami, and Y. Hatsugai, *Prog. Theor. Exp. Phys.* **2020**, 12A109 (2020).
- [68] P. Delplace, T. Yoshida, and Y. Hatsugai, *Phys. Rev. Lett.* **127**, 186602 (2021).
- [69] I. Mandal and E. J. Bergholtz, *Phys. Rev. Lett.* **127**, 186601 (2021).
- [70] C. H. Lee and R. Thomale, *Phys. Rev. B* **99**, 201103(R) (2019).
- [71] D. S. Bognia, A. J. Kruchkov, and R.-J. Slager, *Phys. Rev. Lett.* **124**, 056802 (2020).
- [72] K. Zhang, Z. Yang, and C. Fang, *Phys. Rev. Lett.* **125**, 126402 (2020).
- [73] N. Okuma, K. Kawabata, K. Shiozaki, and M. Sato, *Phys. Rev. Lett.* **124**, 086801 (2020).
- [74] T. Yoshida, T. Mizoguchi, and Y. Hatsugai, *Phys. Rev. Res.* **2**, 022062 (2020).
- [75] R. Okugawa, R. Takahashi, and K. Yokomizo, *Phys. Rev. B* **102**, 241202(R) (2020).
- [76] K. Kawabata, M. Sato, and K. Shiozaki, *Phys. Rev. B* **102**, 205118 (2020).
- [77] L. Jin and Z. Song, *Phys. Rev. A* **80**, 052107 (2009).
- [78] T. E. Lee, *Phys. Rev. Lett.* **116**, 133903 (2016).
- [79] P. San-Jose, J. Cayao, E. Prada, and R. Aguado, *Sci. Rep.* **6**, 21427 (2016).
- [80] Y. Xu, S.-T. Wang, and L.-M. Duan, *Phys. Rev. Lett.* **118**, 045701 (2017).
- [81] V. Kozii and L. Fu, [arXiv:1708.05841](https://arxiv.org/abs/1708.05841).
- [82] A. A. Zyuzin and A. Y. Zyuzin, *Phys. Rev. B* **97**, 041203(R) (2018).
- [83] T. Yoshida, R. Peters, and N. Kawakami, *Phys. Rev. B* **98**, 035141 (2018).
- [84] H. Shen and L. Fu, *Phys. Rev. Lett.* **121**, 026403 (2018).
- [85] M. Papaj, H. Isobe, and L. Fu, *Phys. Rev. B* **99**, 201107(R) (2019).
- [86] T. Matsushita, Y. Nagai, and S. Fujimoto, *Phys. Rev. B* **100**, 245205 (2019).
- [87] Y. Michishita and R. Peters, *Phys. Rev. Lett.* **124**, 196401 (2020).
- [88] A. Guo, G. J. Salamo, D. Duchesne, R. Morandotti, M. Volatier-Ravat, V. Aimez, G. A. Siviloglou, and D. N. Christodoulides, *Phys. Rev. Lett.* **103**, 093902 (2009).
- [89] C. E. Rüter, K. G. Makris, R. El-Ganainy, D. N. Christodoulides, M. Segev, and D. Kip, *Nat. Phys.* **6**, 192 (2010).
- [90] A. Regensburger, C. Bersch, M.-A. Miri, G. Onishchukov, D. N. Christodoulides, and U. Peschel, *Nature (London)* **488**, 167 (2012).

- [91] B. Zhen, C. W. Hsu, Y. Igarashi, L. Lu, I. Kaminer, A. Pick, S.-L. Chua, J. D. Joannopoulos, and M. Soljacic, *Nature (London)* **525**, 354 (2015).
- [92] A. U. Hassan, B. Zhen, M. Soljačić, M. Khajavikhan, and D. N. Christodoulides, *Phys. Rev. Lett.* **118**, 093002 (2017).
- [93] H. Zhou, C. Peng, Y. Yoon, C. W. Hsu, K. A. Nelson, L. Fu, J. D. Joannopoulos, M. Soljačić, and B. Zhen, *Science* **359**, 1009 (2018).
- [94] K. Takata and M. Notomi, *Phys. Rev. Lett.* **121**, 213902 (2018).
- [95] T. Ozawa, H. M. Price, A. Amo, N. Goldman, M. Hafezi, L. Lu, M. C. Rechtsman, D. Schuster, J. Simon, O. Zilberberg, and I. Carusotto, *Rev. Mod. Phys.* **91**, 015006 (2019).
- [96] L. Xiao, T. Deng, K. Wang, G. Zhu, Z. Wang, W. Yi, and P. Xue, *Nat. Phys.* **16**, 761 (2020).
- [97] S. Weidemann, M. Kremer, T. Helbig, T. Hofmann, A. Stegmaier, M. Greiter, R. Thomale, and A. Szameit, *Science* **368**, 311 (2020).
- [98] T. Hofmann, T. Helbig, F. Schindler, N. Salgo, M. Brzezińska, M. Greiter, T. Kiessling, D. Wolf, A. Vollhardt, A. Kabaši, C. H. Lee, A. Bilušić, R. Thomale, and T. Neupert, *Phys. Rev. Res.* **2**, 023265 (2020).
- [99] T. Helbig, T. Hofmann, S. Imhof, M. Abdelghany, T. Kiessling, L. W. Molenkamp, C. H. Lee, A. Szameit, M. Greiter, and R. Thomale, *Nat. Phys.* **16**, 747 (2020).
- [100] T. Yoshida and Y. Hatsugai, *Phys. Rev. B* **100**, 054109 (2019).
- [101] A. Ghatak, M. Brandenbourger, J. van Wezel, and C. Coulais, *Proc. Natl. Acad. Sci. USA* **117**, 29561 (2020).
- [102] C. Scheibner, W. T. M. Irvine, and V. Vitelli, *Phys. Rev. Lett.* **125**, 118001 (2020).
- [103] T. Yoshida, K. Kudo, and Y. Hatsugai, *Sci. Rep.* **9**, 16895 (2019).
- [104] W. Xi, Z.-H. Zhang, Z.-C. Gu, and W.-Q. Chen, *Sci. Bull.* **66**, 1731 (2021).
- [105] T. Yoshida, K. Kudo, H. Katsura, and Y. Hatsugai, *Phys. Rev. Res.* **2**, 033428 (2020).
- [106] C.-X. Guo, X.-R. Wang, C. Wang, and S.-P. Kou, *Phys. Rev. B* **101**, 144439 (2020).
- [107] N. Matsumoto, K. Kawabata, Y. Ashida, S. Furukawa, and M. Ueda, *Phys. Rev. Lett.* **125**, 260601 (2020).
- [108] Q. Zhang, W.-T. Xu, Z.-Q. Wang, and G.-M. Zhang, *Commun. Phys.* **3**, 209 (2020).
- [109] C.-X. Guo, X.-R. Wang, and S.-P. Kou, *Europhys. Lett.* **131**, 27002 (2020).
- [110] H. Shackleton and M. S. Scheurer, *Phys. Rev. Res.* **2**, 033022 (2020).
- [111] K. Yang, S. C. Morampudi, and E. J. Bergholtz, *Phys. Rev. Lett.* **126**, 077201 (2021).
- [112] D.-W. Zhang, Y.-L. Chen, G.-Q. Zhang, L.-J. Lang, Z. Li, and S.-L. Zhu, *Phys. Rev. B* **101**, 235150 (2020).
- [113] T. Liu, J. J. He, T. Yoshida, Z.-L. Xiang, and F. Nori, *Phys. Rev. B* **102**, 235151 (2020).
- [114] Z. Xu and S. Chen, *Phys. Rev. B* **102**, 035153 (2020).
- [115] L. Pan, X. Wang, X. Cui, and S. Chen, *Phys. Rev. A* **102**, 023306 (2020).
- [116] S. Mu, C. H. Lee, L. Li, and J. Gong, *Phys. Rev. B* **102**, 081115(R) (2020).
- [117] C. H. Lee, *Phys. Rev. B* **104**, 195102 (2021).
- [118] S.-B. Zhang, M. M. Denner, T. Bzdusek, M. A. Sentef, and T. Neupert, *Phys. Rev. B* **106**, L121102 (2022).
- [119] K. Kawabata, K. Shiozaki, and S. Ryu, *Phys. Rev. B* **105**, 165137 (2022).
- [120] S. Tsubota, H. Yang, Y. Akagi, and H. Katsura, *Phys. Rev. B* **105**, L201113 (2022).
- [121] F. Qin, R. Shen, and C. H. Lee, [arXiv:2202.10481](https://arxiv.org/abs/2202.10481).
- [122] T. Orito and K.-I. Imura, *Phys. Rev. B* **105**, 024303 (2022).
- [123] T. Tomita, S. Nakajima, I. Danshita, Y. Takasu, and Y. Takahashi, *Sci. Adv.* **3**, e1701513 (2017).
- [124] Y. Takasu, T. Yagami, Y. Ashida, R. Hamazaki, Y. Kuno, and Y. Takahashi, *Prog. Theor. Exp. Phys.* **2020**, 12A110 (2020).
- [125] T. Yoshida and Y. Hatsugai, *Phys. Rev. B* **104**, 075106 (2021).
- [126] In the literature, there are two types of synthetic dimensions. Ref. [35] regards internal degrees of freedoms of particles as synthetic dimensions, while Ref. [33] regards periodic parameters as synthetic dimensions. By making use of the latter type of synthetic dimensions, two-dimensional topology has been studied for a system in one spatial dimension [36,37]. Following these works, we regard the parameter θ as a synthetic dimension and discuss one-dimensional non-Hermitian topology for the quantum dot.
- [127] In the case of a synthetic dimension, one does not have to consider the thermodynamic limit, which significantly simplifies the analysis.
- [128] Instead of w and w_s , one can also use w_\uparrow and w_\downarrow , which are rewritten as $2w_\uparrow = w + 2w_s$ and $2w_\downarrow = w - 2w_s$. The winding number w_\uparrow (w_\downarrow) can be computed in a way similar to Eq. (3) by replacing h in the one-body Hamiltonian with the up-spin (down-spin) sector h_\uparrow (h_\downarrow).
- [129] We note that introducing additional terms makes other subsectors irrelevant. For instance, adding the term $\mu(\hat{N} - 2)$ with $\mu \in \mathbb{C}$ to Eq. (1) can make subsectors labeled by $N = 0, 1, 3, 4$ irrelevant to the topology for $E_{\text{ref}} = 0$.
- [130] Equation (5) indicates that the topology characterized by a finite value of the many-body winding number is robust against interactions. Its robustness can be explicitly checked for $W_{(2,1)} = 1$ and $W_{(2,1)} = 2$. For $W_{(2,1)} = 1$, the robustness of the topology can be seen in Figs. 2(a) and 2(b). Figure 2(a) indicates that the topology is characterized by $W_{(2,1)} = 1$ for $E_{\text{ref}} = i$ in the absence of the interactions. Figure 2(b) indicates that this nontrivial topology is maintained in the presence of the interactions. The topology characterized by $W_{(2,1)} = 2$ can be discussed by replacing h , whose robustness is discussed in Sec. A 2.
- [131] At the noninteracting level, the fragility of the skin effect against spin-flipping terms was discussed in Ref. [55]. In that previous work, the one-body term keeps the point-gap topology nontrivial, while our two-body interactions destroy the nontrivial topology.